climate

MDPI

Article

Evaluation of the Urban Microclimate in Catania Using Multispectral Remote Sensing and GIS Technology

Michele Mangiameli [1,*], Giuseppe Mussumeci [1] and Antonio Gagliano [2]

[1] Department of Civil Engineering and Architecture (DICAR), University of Catania, Viale Andrea Doria, 6, 95125 Catania, Italy; giuseppe.mussumeci@unict.it
[2] Department of Electrical, Electronics and Computer Engineering (DIEEI), University of Catania, Viale Andrea Doria, 6, 95125 Catania, Italy; antonio.gagliano@unict.it
* Correspondence: michele.mangiameli@unict.it

Abstract: This study focuses on the determination and examination of both the Land Surface Temperature (LST) and the atmospheric temperature in the city of Catania Sicily (Italy), through freely available satellite remote sensing images from the Sentinel-2 and MODIS missions. Satellite images were processed as raster data in free and open-source GIS environments. The GIS software allows the retrieval, processing of the satellite images for the estimation of the LST and the atmospheric temperature with a very coarse spatial resolution. In particular, the proposed procedure allows increasing the spatial resolution of satellite images, from 250 m (LRES) to 10 m (HRES) through the principle of "Disaggregation of thermal images". The analysis provided georeferenced maps which show the LST, as well as the atmospheric temperature within the investigated area with a very fine resolution, 10 m. Such spatial resolution reveals evident correlations between areas with different urban densities and their microclimate. An important result of this study is that significant LST differences can be observed during both day (15–17 °C) and night (2–3 °C) between green and built-up areas. The outcomes of this study highlight the effectiveness of the combined use of satellite remote sensing and GIS for analyzing the thermal response of urbanized areas with different built density.

Keywords: urban microclimate; remote sensing; GIS; LST; NDVI

Citation: Mangiameli, M.; Mussumeci, G.; Gagliano, A. Evaluation of the Urban Microclimate in Catania Using Multispectral Remote Sensing and GIS Technology. *Climate* **2022**, *10*, 18. https://doi.org/10.3390/cli10020018

Academic Editor: Constantinos Cartalis

Received: 24 November 2021
Accepted: 24 January 2022
Published: 5 February 2022

1. Introduction

Urban microclimate is defined as the local climate observed in urban areas, which can be significantly different from the climate of the surrounding rural areas. Temperature is one of the climatic parameters that differentiates within urban areas and it is associated with the Urban Heat Island (UHI) effect, which may significantly impact on human health. Various studies report average temperature differences of ~2–4 °C, which can even reach 10 °C in extreme cases [1–5].

There are several factors that affect the microclimate of an urban area. The increase of both daily and night temperatures contributes to the severe degradation of the urban microclimate and air quality, with higher pollution levels, that may increase the heat-related deaths/illnesses (e.g., heat cramps, respiratory difficulties, heat exhaustion, etc.) [2–5]. The determining factors in the formation of the urban microclimate are the absorption coefficient of the surfaces, the presence of vegetation and bodies of water, which favour the evapotranspiration, the density of the inhabited centre, the sky view, the vehicular traffic and the use of heating/cooling systems [6]. At the same time, replacing natural ground cover with concrete, infrastructure, and industrial activities results in the elimination of natural cooling effects [7].

Moreover, the presence of high buildings and narrow streets can heat the air trapped between them. Typically, in cities, narrow streets and high buildings create urban canyons

where smaller part of the sky is visible decreasing the possibility of night cooling. This particular phenomenon is described by the Sky View Factor(SVF) which influences the formation of UHI [8]. Conversely, the urban microclimate is mitigated by the presence of large bodies of water, sea breeze phenomenon and vegetation that favours evapotranspiration [8–10].

Anthropogenic solutions to mitigate the urban microclimate effect include the installation of Photovoltaic (PV) pavements, especially in the roadway and parking lots that occupy large urban areas. Indeed, it has been shown that the adoption of PV pavements is an efficient solution not only for alleviating the urban microclimate effects but also for generating renewable energy [11,12]. The impact of PV plants on building surface temperature, urban-canyon air temperature and energy fluxes was evaluated in [13,14]. Recent studies have also found that high albedo materials, used for urban elements and homes, green areas and urban inland water bodies assist in mitigating the urban microclimate [15].

The Land Surface Temperature (LST), which is the brightness temperature of the land surface, is close to the real temperature on the surface but has a strong relationship with air temperature, being an indicator for urban microclimate [16,17]. LST measurements are commonly retrieved from remotely sensed thermal-infrared (TIR) data in order to detect the upwelling thermal radiance, allowing the examination of the natural and human-induced changes impact on surface temperatures [18]. LST is influenced by different aspects, including albedo, vegetation cover and soil moisture, atmospheric temperature and humidity, clouds and large aerosol particles such as dust [19].

Several studies are based on satellite-derived vegetation indices calculated from single spectral bands (e.g., NDVI, IBI, partial least square, etc.), confirming their effectiveness in the detection and continuous monitoring of UHI [20]. For instance, Landsat TM/ETM+/OLI thermal bands have been used to map urban heat islands over the Southern region of Cairo Governorate (Egypt), in Cairo and Giza, which have been subject to uncontrolled expansion over the past 50 years, and thus identify a correlation between major urban microclimate and urbanization [21–23]. Air temperature for 22 years was also analyzed in the city of Athens [24], highlighting temperature variations caused by natural processes and anthropogenic activities, and finding a correlation between city growth and the average minimum temperature increase.

The use of the GIS software has been proven to be a valuable tool for the processing of remote sensing data and the management of space-time data in different areas of engineering, from environmental monitoring to archaeology [25–29]. GIS has been also used as a simulation environment to calculate the maximum intensity of urban heat islands based on urban geometry data in two or three dimensions. Starting from the correlation between the vertical elevation of urban morphology and urban microclimate, GIS and artificial neural network have been used to predict the spatial distribution of urban microclimate considering a terrain correction integrated with other morphological parameters [30].

This study aims at presenting a novel GIS-based procedure for the detection and analysis of the variation of the LST and atmospheric temperature using freely available satellite images, which can provide extensive and reliable information about urban microclimate and their relationship with the economic, social and environmental factors [31]. The GIS software allows the retrieval, processing of the satellite images for the estimation of the LST and the atmospheric temperature with a very fine spatial resolution. In particular, the proposed procedure allows increasing the spatial resolution of satellite images, from 250 m (LRES) to 10 m (HRES) through GIS software elaborations.

Intending to test the proposed procedure, this research presents an application in Catania, a city located on the eastern coast of Sicily (Italy), where, like other coastal cities, the Urban Microclimate (UMC) is evident and persistent during summer [31–35], but no previous studies have been conducted. Catania is one of the most important Italian cities, among the top eight cities, with a population of about 300,000 people. Moreover, Catania is characterized by a particular geographic location: it is bordered by the sea at South-Est and by the Etna volcano at North, and a wide flat agricultural area at South West, namely the

"Piana di Catania", which creates a very particular topography affecting the microclimate of the city.

The paper is organized as follows: Section 1 presents a selection of literature studies regarding the evaluation of UMC through satellite analysis; Section 2 illustrates the procedure followed for the management of the available satellite data into the GIS environment; Section 3 presents the results, which consists of both the analysis of the meteorological data derived by fixed weather stations (Section 3.1) and the maps of NDVI and LST (Section 3.2) and air temperature (Section 3.3); Section 4 discusses the main findings and summarizes the work.

2. Materials and Methods

2.1. Satellite Data

The satellite images are obtained from the NASA's TERRA (EOS AM-1; https://terra.nasa.gov/, accessed on 7 July 2020) and Aqua (EOS PM-1; https://aqua.nasa.gov/, accessed on 7 July 2020) satellites equipped with Moderate Resolution Imaging Spectroradiometer (MODIS), and by the Sentinel-2 satellite of the Copernicus program, downloaded using the QGIS SCP plug-in (https://earthdata.nasa.gov/, accessed on 7 July 2020).

Terra MODIS and Aqua MODIS observe the entire Earth's surface every 1 or 2 days, acquiring data in 36 spectral bands.

The SENTINEL-2 Multispectral Instrument (MSI) is characterized by:

- Four bands with spatial resolution of 10 m.
- Six bands with spatial resolution of 20 m.
- Three bands with spatial resolution of 60 m.

These images have been processed using Quantum GIS (or QGIS), which is a free and open-source cross-platform GIS software that supports viewing, editing, and analysis of geographic data. For our purpose, QGIS was used to manage the satellite images as georeferenced rasters and calculate quantitative environmental indices.

2.2. Normalized Difference Vegetation Index

The Normalized Difference Vegetation Index (NDVI) has been calculated in a GIS environment using MODIS satellite images. The NDVI is a vegetation index based on the proportion of reflected light in the visible red spectra (VIR), which is absorbed by plants for photosynthesis, and reflected light in the Near-Infrared (NIR) spectra, which is usually not absorbed by plants as wavelengths are too long for photosynthesis. It is widely used to forecast agricultural production, advising on the greenness of biomes [31].

The NDVI ranges from –1 to 1: negative values correspond to water, while values close to zero (–0.1 to 0.1) correspond to areas of rock, sand, or snow. Moderate NDVI values correspond to a grassland area (from 0.2 to 0.4). High NDVI values (from 0.6 to 0.9) indicate dense vegetation (i.e., temperate, and tropical forests or crops at peak growth stage). The NDVI is determined by the difference in the intensities of reflected light in the red and infrared range divided by the sum of these intensities [36,37]:

$$\mathrm{NDVI} = \left(\frac{\mathrm{NIR} - \mathrm{VIR}}{\mathrm{NIR} + \mathrm{VIR}}\right) \quad (1)$$

In this study, the MODIS Near Real-Time (NRT) level-2G Global 250 m product (MOD09GQ), which provides bands B1 (620–670 nm) and B2 (841–876 nm) at a 250-m resolution, was used to calculate the NDVI_{250}, where the subscript 250 indicates the spatial resolution. The NDVI_{10} was also derived by the Sentinel-2 Multi-Spectral Instrument (MSI) imagery with 10 m spatial resolutions using the spectral bands B4 (VNIR) and B8 (NIR).

2.3. Weather Data

Data derived from the satellite images were compared with the weather data measured by three weather stations (WSs), namely WS1, WS2 and WS3, sited within the urban and suburban areas of Catania.

Catania is bordered to the East by the Ionian Sea, to North by Etna volcano, and to the West and South by agricultural land oasis (Figure 1a). The position of the urban centre of Catania (yellow circle) and the location of the three WSs are shown in Figure 1b.

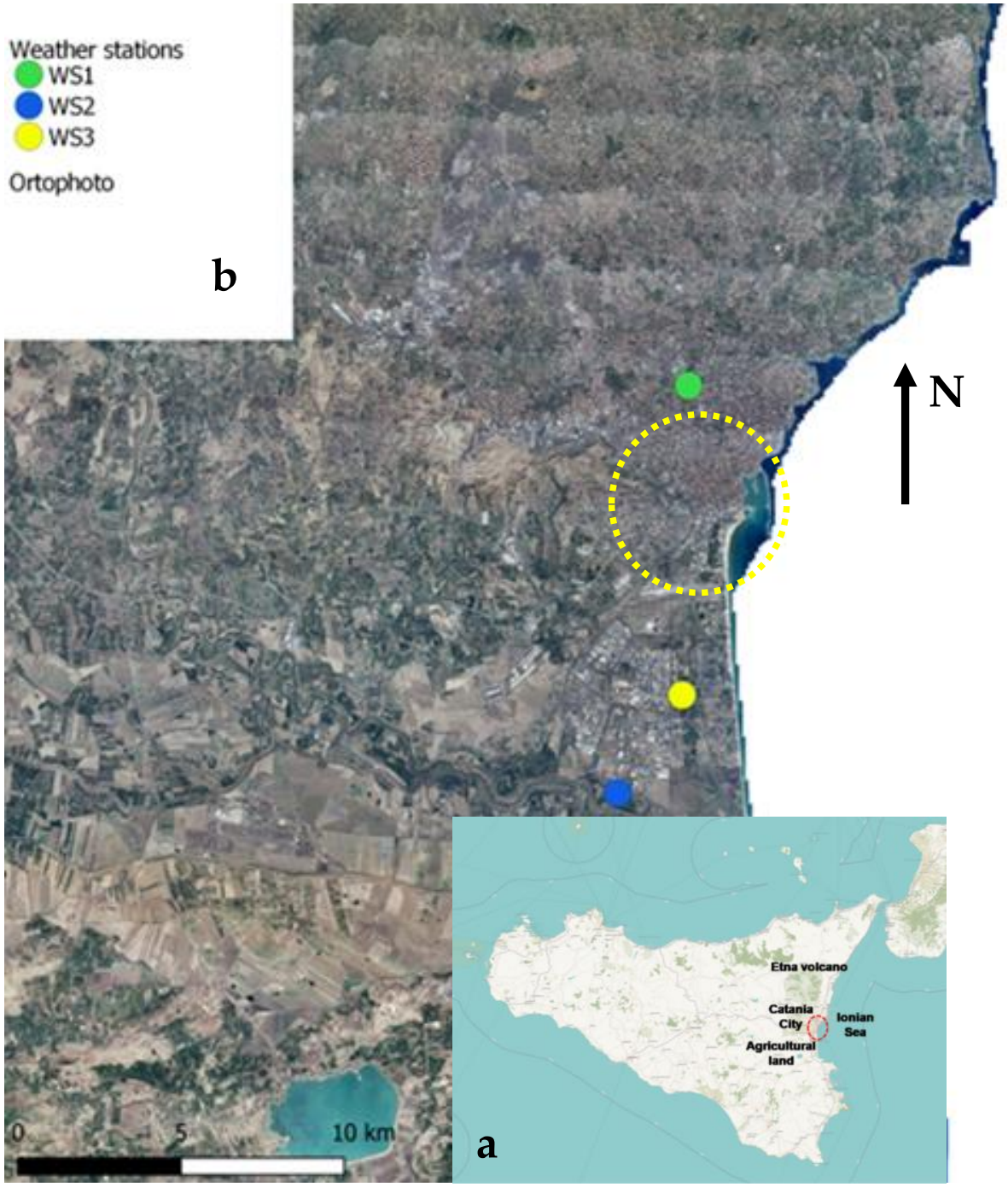

Figure 1. (**a**) Geographic position of Catania city, object of the study; (**b**) localization of the urban centre of Catania (yellow circle) and the three WSs.

The WS1 is owned by the Department of Electric, Electronics and Computer Engineering of the University of Catania and is located in the north part of the city, within the university campus, near an almost densely built area and important busy street. The weather data recorded are mainly used for the analysis of the performances of the solar system (PV and PVT plants). The WS2 is owned by the ENEL Green Power S.p.A.-Innovation Lab di Catania anddd is placed nearby the industrial area south of town, which is assumed to be rural. The WS3 is owned by the Sicilian Agrometeorological Information Service (SIAS), which provide the official network of the Sicily region and is located south of town in a rural area with very low built-up density nearby the urban centre.

2.4. Land Surface Temperature

The Land Surface Temperature (LST) is the temperature of the outermost layer of the earth's surface and is measured along the direction of the remote acquisition sensor. It is derived from the top-of-atmosphere brightness temperatures retrieved from the infrared spectral channels of geostationary satellites (Meteosat Second Generation, GOES, MTSAT/Himawari). Since the LST indicates the redistribution of energy into latent and sensible heat fluxes, it gives fundamental information on the surface energy and water balances [34,35].

The MOD11A1 product (https://lpdaac.usgs.gov/products/mod11a1v006, accessed on 7 July 2020) provides daily per-pixel Land Surface Temperature and Emissivity (LST&E) with 1 kilometer of spatial resolution in a 1200 km by 1200 km grid (https://lpdaac.usgs.gov/products/mod11a1v006, accessed on 7 July 2020). Thus, following the procedure proposed by Baghdadi [38] the MOD11 LST data (https://modis.gsfc.nasa.gov/data/dataprod/mod11.php, accessed on 7 July 2020), with 1 km of spatial resolution, are converted to temperature (in K) using the QGIS raster calculator tool as follows:

$$LST_{1000} = MOD11 * 0.02 \quad (2)$$

To avoid inconsistent values of temperature, the constrain that LST has to be higher than 273 K is imposed [39].

Since the spatial resolution and the area covered by the MODIS and Sentinel images are different, the QGIS "Align" tool is used to obtain images with the same areal extent and the same number of pixels, resized from images with 10 m (High RESolution—HRES) to 1000 m Low RESolution—LRES) of spatial resolution images and vice-versa. The "Align" tool allows to line up and subset different images, giving them the same spatial resolution by resizing LRES to HRES images. To avoid misleading results, the images are then resized to their original spatial resolution (250 m for $NDVI_{LRES}$ and 1000 m for LST_{LRES}) and deprived of the negative values, not altering the resolution, considering these values as "no data" in the raster calculator tool.

To combine the low spatial resolution MODIS thermal images with the higher resolution MSI visible and near-infrared images (VNIR) that come with high spatial resolution, we used the principle of "Disaggregation of thermal images" [40–45]. The relationship between LST and NDVI is obtained by fitting a linear regression to the observed data, which gives rise to the following equation [39]:

$$LST = a + b * NDVI \quad (3)$$

where the coefficients a and b are determined through a linear regression model. The coefficients of the linear regression that correlate $NDVI_{LRES}$ ($NDVI_{1000}$) and $NDVI_{250}$ were obtained using the GRASS toolbox available in QGIS [39]:

$$NDVI_{1000} = 0.15 + 0.81 * NDVI_{250} \quad (4)$$

In this way, it is possible to determine the $NDVI_{1000}$ as a function of $NDVI_{250}$.

After setting the cell size of $NDVI_{LRES}$ to 1 km, i.e., the spatial resolution of LST_{LRES}, through the GRASS "resamp" command, the same procedure is used to correlate LST_{LRES} with $NDVI_{LRES}$ [39]. The coefficients of the linear regression that correlate LST_{LRES} (LST_{1000}) with $NDVI_{LRES}$ ($NDVI_{1000}$) are found through:

$$LST_{1000} = 321.5 - 8.5 * NDVI_{1000} \quad (5)$$

The LST_{HRES} (LST_{10}) is calculated as a function of the $NDVI_{10}$ using the same coefficients of Equation (5) [40]:

$$LST_{10} = 321.5 - 8.5 * NDVI_{10} \quad (6)$$

Recent studies have demonstrated a correlation between observation of atmospheric temperature and estimated temperature from satellite data [39,42–47].

For the calculation of atmospheric temperature Ta, the regression model presented by Kloog et al. [48] has been adopted due to its wide field of application.

Indeed, such model relates the atmospheric temperature with the land surface temperature, the elevation of the area, NDVI, and the percentage of urban area in the grid as follows:

$$T_a = (M_1 * LST) + (M_2 * UrbanPercent) + (M_3 * Elevation) + (M_4 * NDVI) + B \quad (7)$$

where

- M_1 is the LST slope,
- M_2 is the sum of the fixed and random Urban Percent slopes.
- M_3 is the sum of the fixed and random elevation slopes.
- M_4 is the sum of the fixed and random NDVI slopes.
- LST is the LST_{HRES} derived by Equation (6).
- Urban Percent is the percentage of urban area in the grid.
- Elevation is calculated from DEM (Digital Elevation Model).
- NDVI is the $NDVI_{HRES}$.
- B is a datum obtained as the sum of the fixed intercepts and random intercepts.

The elevation is calculated from the DEM of the investigated area within the GIS software. The reliability of the Ta calculated, determined as raster data in the GIS environment, is performed making a comparison with the temperatures measured by three fixed weather stations, called WS1, WS2 and WS3, installed within the investigated area (see Figure 1). Further information on such weather stations is provided in Section 3.1.

It is worth noting that Equation (7) is a statistically derived equation that has local/regional applicability, since LST depends on urban morphology, urban functions and urban fabric. Thus, when it is used in areas that have different urban characteristics, it is compulsory to investigate the robustness of the results obtained. In this context, assuming possible variability of the regression coefficients between +/−10% and LST temperature of 50 °C, which is close to the maximum values observed, an average fluctuation of the air temperatures in the range +/−2.2 °C, with a maximum variation of +/−3.4 °C, was observed.

We would underline the application of Equation (7), within this study, gives rise to atmospheric temperatures lower than the LST at midday and higher at night, as expected. Finally, a preliminary assessment on the reliability of the application of Equation (7) in the investigated area is presented. Figure 2 represents the flowchart of the proposed methodology, showing the datasets used, the processing stage and the output.

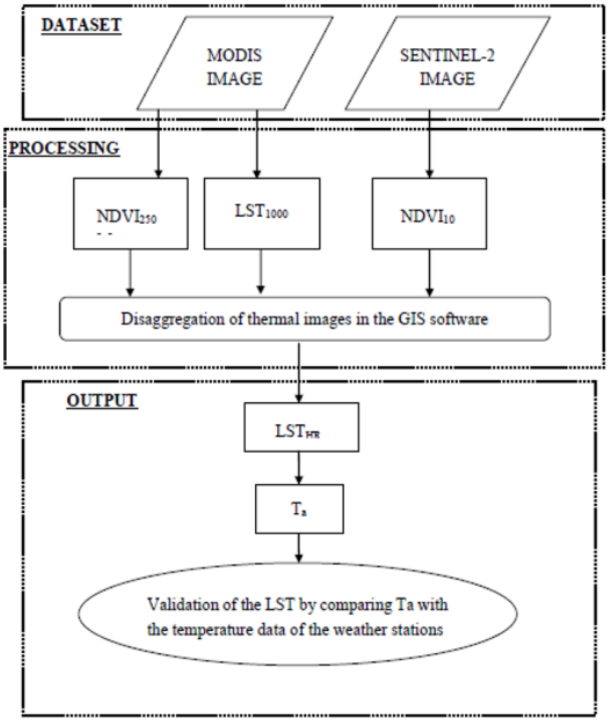

Figure 2. Flowchart of the methodology used.

2.5. Case Study

The procedure described in the previous sections is applied to the urban area of Catania, (Italy) which extends in an area of 182.9 km^2, (longitude: 15.07435, latitude: 37.51563). Figure 3 shows the ortophoto of Catania, where some areas of interest are indicated.

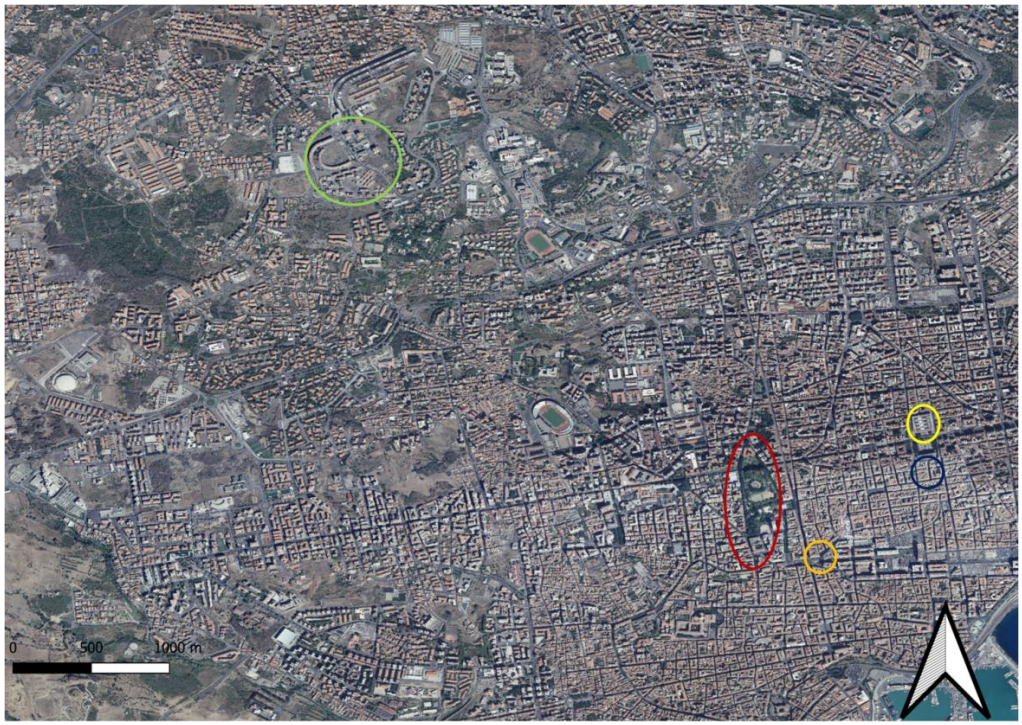

Figure 3. Ortophoto of Catania city, red circle highlights Villa Bellini, yellow circle the courthouse, blue circle the skyscraper, orange circle Stesicoro square and green circle is San Nullo district.

The procedure to determine the LST, as well as the atmospheric temperature in the GIS software consists of the following steps:

- Selection of the days to analyse based on the availability of both weather station and satellite data.
- Processing of MODIS and SENTINEL-2 satellite images in a GIS environment.
- Application to the investigated area.
- Analysis of the atmospheric temperatures.

This study presents the comparison between air temperatures calculated through the proposed procedure and the data measured at the three weather stations during 12 days comprized between July–August 2007 with a cloud coverage <0.25% (Table 1).

Table 1. Overpass time of the satellite for the twelve investigated days. Greenwich Mean Time (GMT).

Days	Daytime	Nighttime
4 July 2017	10:36	21:36
9 July 2017	10:54	22:00
12 July 2017	11:24	22:20
14 July 2017	11:12	22:18
22 July 2017	10:24	21:30
29 July 2017	10:30	21:36
3 August 2017	10:48	21:54
11 August 2017	11:36	22:42
16 August 2017	10:18	21:18
18 August 2017	11:42	22:48
26 August 2017	10:54	22:00
28 August 2017	10:42	21:48

3. Results

3.1. Data Measured by the Weather Stations

In this section, the weather station observations are discussed showing the first evidence of temperature difference between areas of different land use during the 12 selected days. In particular, we estimated the maximum, minimum and average temperatures during each day and measured the difference of the minimum temperatures by choosing couples of weather stations, highlighting the average temperature difference during the entire period. The maximum, minimum and average temperatures measured by the weather stations during the 12 days selected are summarized in Table 2.

Looking at the entire period (4 July–28 August), it is observed that for many days the higher daily values of maximum temperature (Tmax), as well as the lower daily minimum temperatures (Tmin) are observed by the WS2. The WS1 and WS3 observed almost similar values of the maximum daily temperature (Tmax). Regarding the Tmin timeseries, the temperatures observed by WS3 are lower than that observed by WS1. This is due to the fact that WS1 is located in an densely built area, WS2 is placed in the industrial area of Catania and WS3 is located in the surrounding rural area.

Table 2. Maximum, minimum and average temperatures (T_{max}, T_{min}, T_{avg}) observed at the three WSs (DIEEI, ENEL, SIAS) during the 12 analyzed days.

Days	WS1-DIEEI (Lat 37.525, Long 15.072)			WS2-ENEL (Lat 37.414, Long 15.047)			WS3-SIAS (Lat 37.441, Long 15.069)		
	T_{max}	T_{min}	T_{avg}	T_{max}	T_{min}	T_{avg}	T_{max}	T_{min}	T_{avg}
4 July 2017	29.2	22.0	25.9	31.5	16.6	25.6	29.7	19.8	25.5
9 July 2017	36.8	24.7	30.5	36.1	18.9	27.6	34.2	24.7	27.5
12 July 2017	39.9	28.2	33.3	42.1	23.7	31.2	40.8	25.5	31.7
14 July 2017	33.2	25.3	29.1	32.4	19.9	27.1	31.1	21.6	27.1
22 July 2017	36.2	25.8	31.7	40.0	21.9	30.8	37.9	23.5	31.3
29 July 2017	33.3	23.3	27.2	32.1	17.6	25.6	30.7	20.6	25.6
3 August 2017	37.5	26.4	32.1	39.1	20.2	28.8	34.2	21.2	28.8
11 August 2017	35.3	26.4	31.2	35.3	22.8	28.8	34.2	24.8	29.0
16 August 2017	31.6	23.7	27.6	31.9	19.9	26.3	30.9	21.6	26.9
18 August 2017	32.8	24.1	28.7	34.1	19.3	27.0	33.5	21.6	27.4
26 August 2017	32.7	23.9	27.8	33.2	18.7	25.9	31.9	21.0	26.2
28 August 2017	32.2	24.1	28.2	33.0	17.9	26.0	31.1	20.0	26.2

To highlight the variation in the minimum temperature at the different weather stations, we performed differences per pair of stations, i.e., WS1–WS2, WS1–WS3 and WS3–WS2, as shown in Figure 4. The minimum temperatures observed at WS1 are 2–6 °C higher than the other two WSs. The average temperature difference (ΔTu-r) between WS1 and WS2 results 5.04 °C with a standard deviation of 0.92 °C, while ΔTu-r between WS1 and WS3 gives rise to 2.98 °C with a standard deviation of 1.1 °C. These values highlight the increase of the air temperature moving from the city centre to the far surroundings, where the WS2 is placed. In light of the above analysis, the differences between daily Tmin measured by the urban weather station WS1, and those measured by the WS1 and WS3 weather stations, could provide preliminary evidence for the heat island intensity

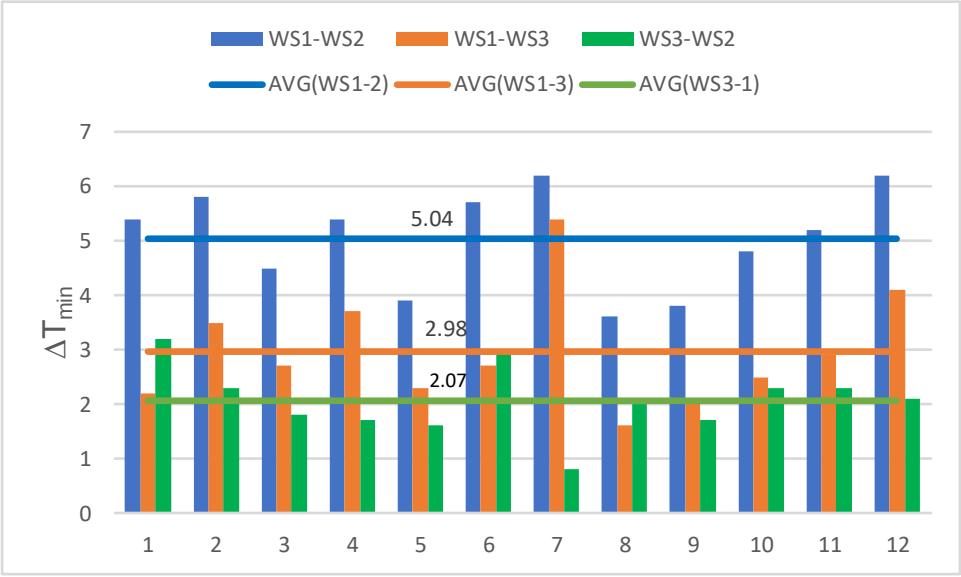

Figure 4. Difference of Tmin between WS1–WS2 (vertical blue bars), WS1–WS3 (vertical orange bars) and WS3–WS2 (vertical green bars) during the 12 selected days (x axis). The horizontal bars indicate the average difference during the entire period.

3.2. NDVI and LST Derived by Satellite Images

In this section, we present the comparison between the NDVI and LST at different spatial resolutions in the urban center of Catania for two selected days, 14 July and 26 August 2017. Moreover, we selected a specific area around "Villa Bellina", where we estimated the high-resolution LST, highlighting its difference between the daytime and nighttime. The same estimates are reported for references buildings/areas of the city.

The raster maps concerning the NDVI and the LST at low (250 m) and high (10 m) spatial resolution on 14 July 2017 are shown in Figure 5. In the LRES image (Figure 5a), the NDVI is fairly invariable in all the area of Catania. In contrast, in the HRES image, many green spots and scattered areas appear. Among these green areas, a very representative site is "Villa Bellini"(red circle), which is an large urban park covering an area of 6.1 ha. The striking level of detail achieved with the HRES image (Figure 5b) can be appreciated by looking at the white elliptic area within the "Villa Bellini", which is represented by NDVI = 0.16. Such a value is reasonable, as this particular area is an arena paved with sand. In general, Figure 5b highlights different vast areas with NDVI lower than 0.3, reflecting the high built density zones of Catania. Similar annotations can be drawn comparing the LRES and HRES LST images (Figure 5c,d), where the purple spots highlight the areas with the lowest LST temperature corresponding to the vegetated area.

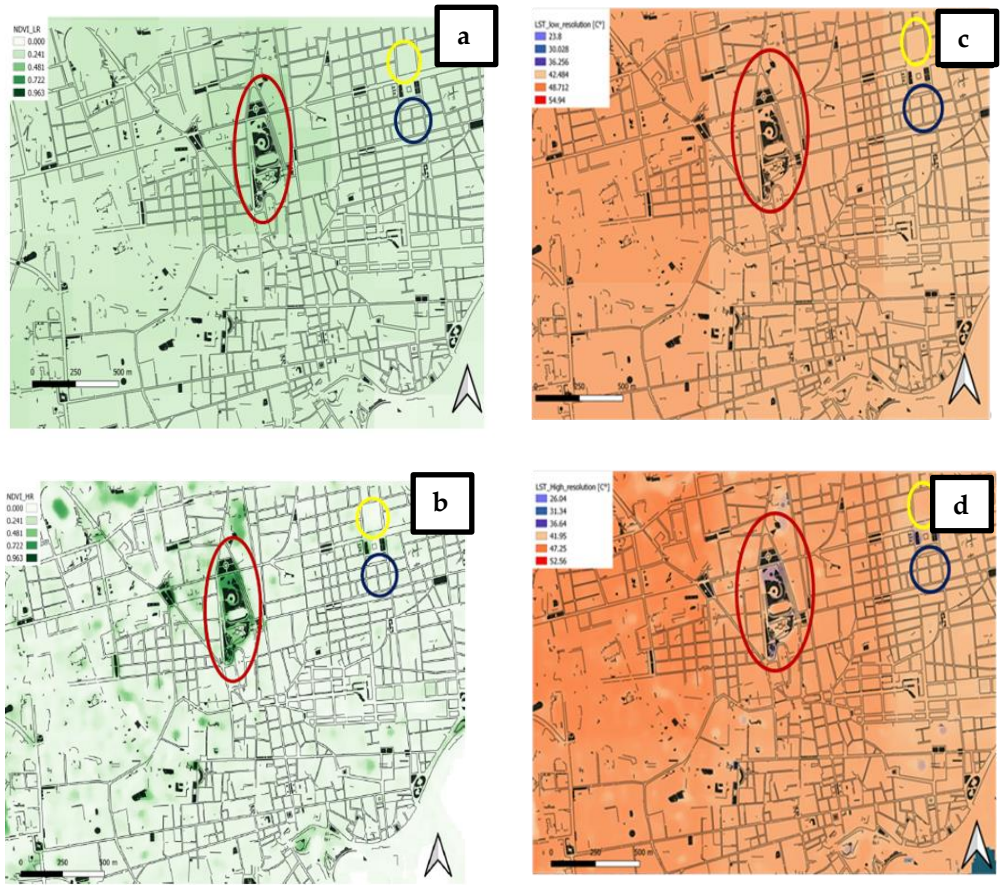

Figure 5. $NDVI_{250}$ (**a**), $NDVI_{10}$ (**b**), LST at low (**c**) and high resolution (**d**) on 14 July 2017. The red circle highlights Villa Bellini, the yellow circle the courthouse and the blue circle the skyscraper.

To further point out the helpfulness of the proposed procedure for obtaining more detailed evaluations on the urban climate, the zonal-statistics raster QGIS tool was applied to the sample area indicated by the yellow box of Figure 6. Within this sample area, the minimum (LST_{min}), maximum (LST_{max}) and average LST (LST_{avg}) temperature were determined. As the zone under investigation is represented by a single pixel, the LRES image (Figure 6) returns a single LST value for the entire area (44 °C). On the contrary,

using the HRES image at 10 meters, the area can be better characterized. Indeed, using the statistical raster tool, we calculated the LST_{min}, LST_{max} and LST_{avg} that result 26.05, 44.92 and 44.39 °C, respectively. To highlight the difference in temperature between the day and nighttime period, we depicted the LST_{10} during two days, on 14 July and 26 August 2017 (Figure 7).

Figure 6. Area subjected to statistical analysis.

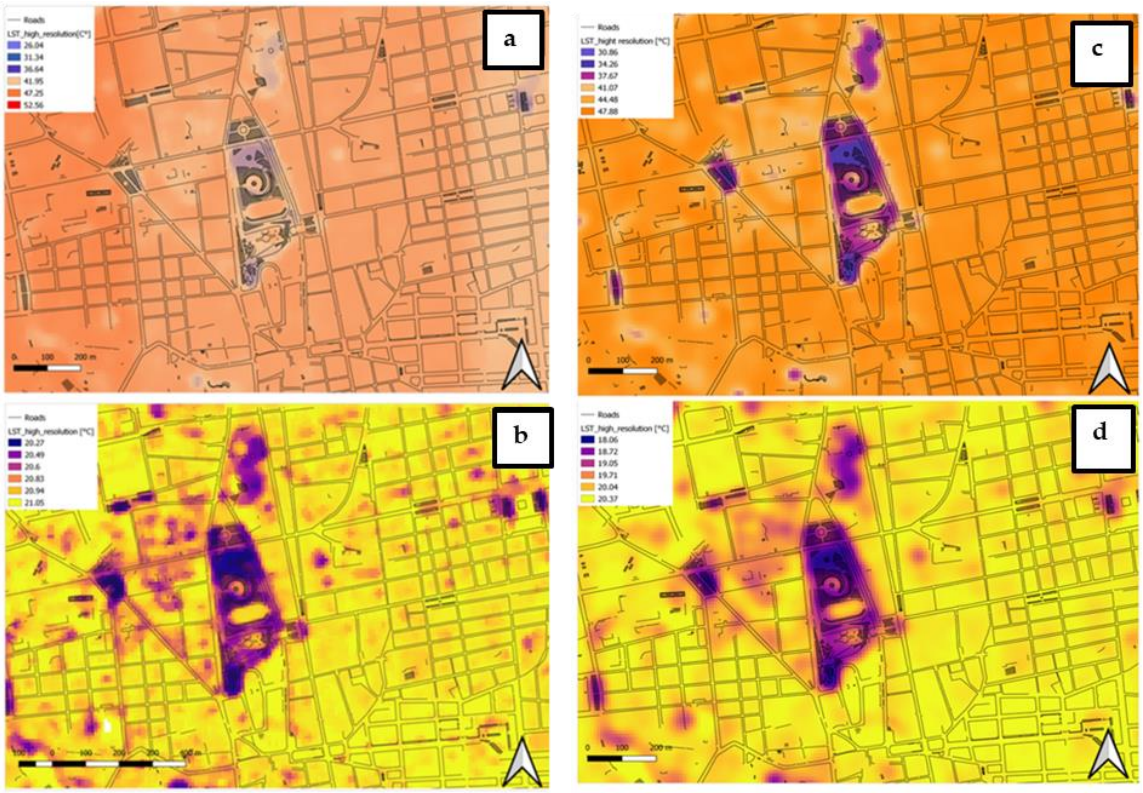

Figure 7. Daytime (**a**) and nighttime (**b**) LST_{10} on 14 July 2017. Daytime (**c**) and nighttime (**d**) LST_{10} on 26 August 2017.

As can be observed, a different thermal behaviour between the green and the paved areas emerges, due to the different albedo coefficients for these two types of surfaces. This effect can be better noticed by looking at the the temperature difference between the green areas and the built-up areas (Figure 8), where the green areas are 2–3 °C cooler than the built-up areas during the night period and even of 15–17 °C during the daytime. As a

result, the green areas, which are low albedo areas allowing reduced absorption of solar radiation, are characterized by cooler LST and atmospheric temperatures. These results confirm the LST is closely related to the city energy use.

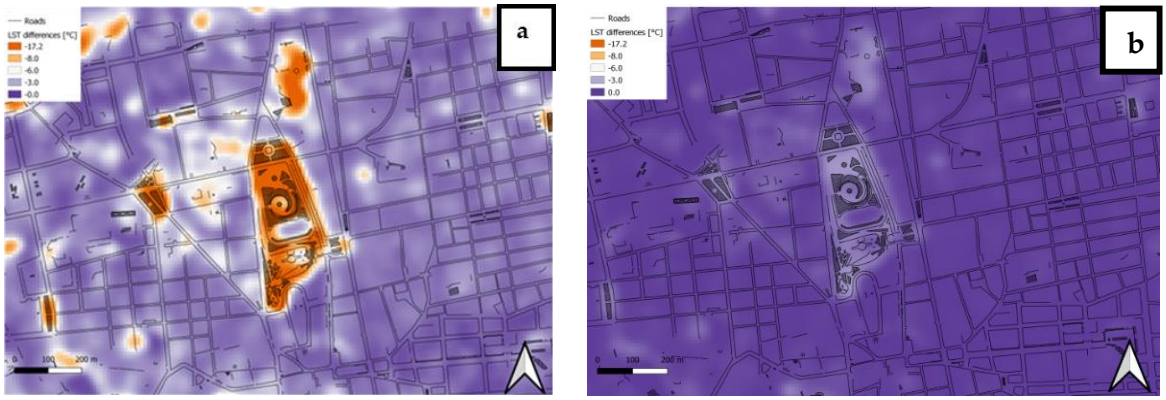

Figure 8. Daytime (**a**) and nighttime (**b**) LST differences on 26 August 2017.

Looking at the atmospheric temperatures measured by the WS1 on these days, the green areas have temperatures 2–3 °C lower than the surrounding areas. Thus, it is possible to assert that the green areas in addition to the evapotranspiration effect, further contribute to cooling down the environment through sensible heat fluxes. On the contrary, the built-up areas have LST temperatures 15–17 °C higher than the atmospheric temperatures. This outcome indicates that the very hot pedestrian surface contributes to the increase of surrounding air temperature. As a further analysis, we considered some reference buildings/areas of Catania ("Villa Bellini", the highest building of the city, namely the skyscraper, and the courthouse) and evaluated the LST during these two days (Table 3).

Table 3. LST for the chosen references buildings/areas on 14 July and 26 August 2017. Temperatures are in °C.

	Daytime Temperature on 14 July	Daytime Temperature on 26 August	Nighttime Temperature on 14 July	Nighttime Temperature on 26 August
Villa Bellini	29	31	20	18
Skyscraper	45	44	21	20
Courthouse	42	45	21	20

3.3. Atmospheric Temperature

In this section, we discuss the satellite-derived atmospheric temperatures during daytime and nighttime and compared them with those measured by the three weather stations. The analyses are performed first for the urban area of Catania and then for two representative areas, i.e., the Stesicoro square and San Nullo district.

The variation of the atmospheric temperature in the central urban area of Catania during day and night is shown in Figure 9. The atmospheric temperature maps allow the identification of cooler areas (blue and purple colors), which coincide with green areas of the investigated region. It is also possible to observe as these cool areas are spread within the city. During the day (Figure 9a), the atmospheric temperature ranges from 23.65 to 34.44 °C, while during the night (Figure 9b), the variation is less evident, with the temperature going from 21.58 to 22.47 °C.

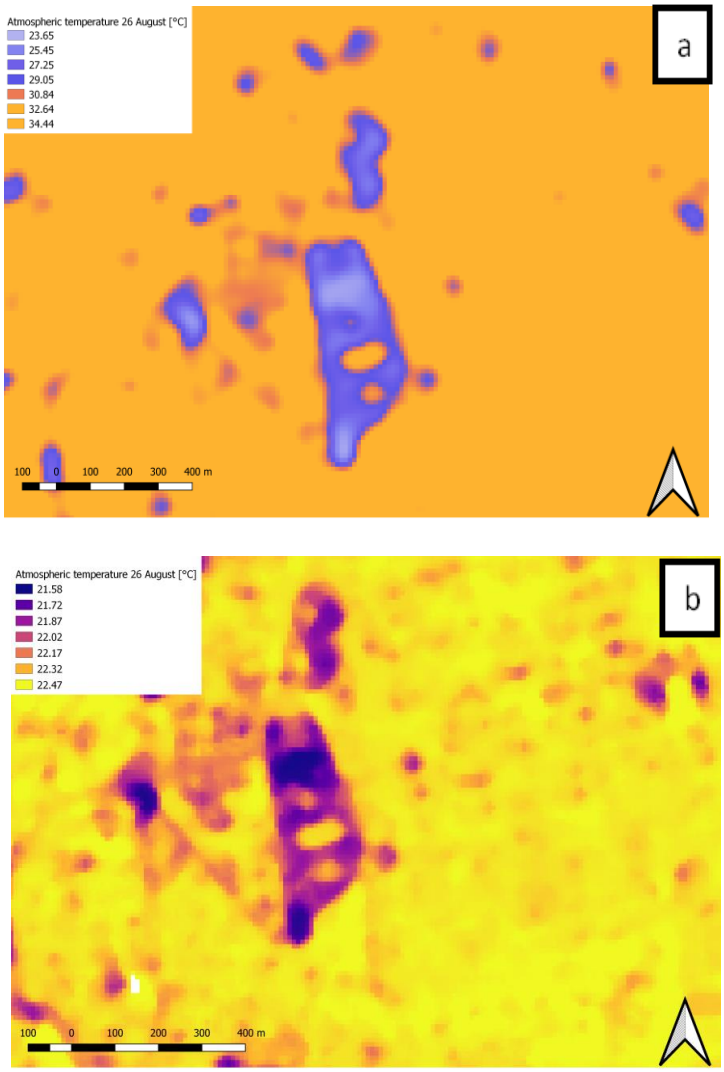

Figure 9. Daytime (**a**) and nighttime (**b**) atmospheric temperature on 26 August 2017.

The analysis of the atmospheric temperature is in agreement with the air temperatures measured by the three weather stations and those determined by the proposed procedure in the same sites. Indeed, an average difference of 0.8 °C and a standard deviation of 0.5 °C is found between the observed (exp) and calculated (sim) atmospheric temperature (Tmax) at WS1, WS2 and WS3 on 14 July and 26 August 2017 (Figure 10). The differences between the simulated and experimental data range from 0.1 to 1.29 °C for WS1 and from 0.89 to 2.31 °C for WS3, while the lowest difference was observed at the position of WS2, being 0.18 and 0.24 °C on 7 July and 26 August, respectively.

The comparison between measured and simulated air temperature highlighted a maximum difference of 2.31 °C. This impreciseness of the prediction is in accordance with the average error, evaluated in the application of Equation (7) as previously pointed out.

Although, the average differences between measured and simulated data are less than 1 °C, it is mandatory to extend the number of observations, both in space and time, with the aim of tuning the regression coefficients of Equation (7), in such a way to derive a new correlations validated within the investigated area. Another fundamental aspect that has to be taken into account is the delay time that relates the time variation of LST and atmospheric temperature, due to the rapid change of LST in comparison with atmospheric temperature.

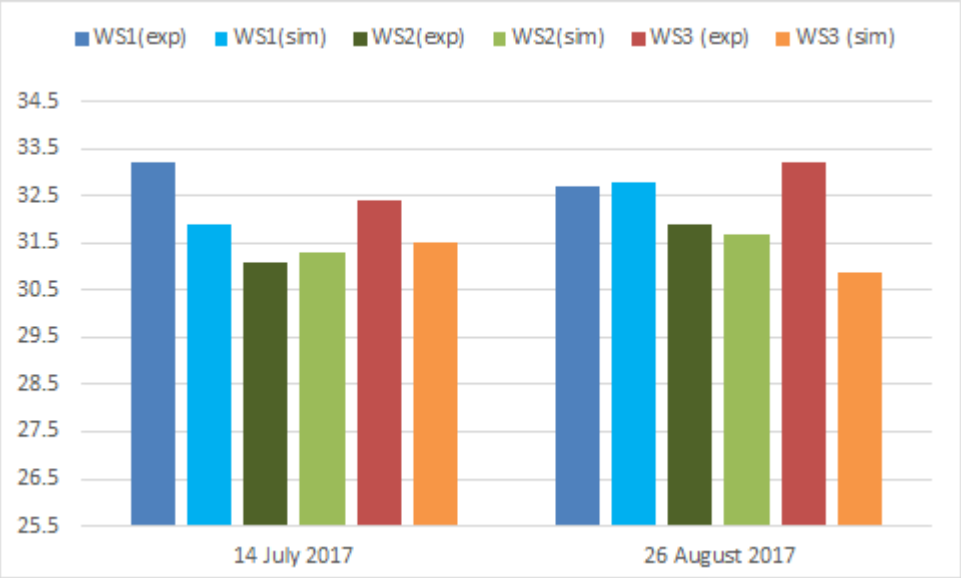

Figure 10. Observed (exp) and calculated (sim) atmospheric temperature (Tmax) at the three weather stations site (WS1, WS2, WS3 as) on 14 July and 26 August 2017.

In order to further illustrate the potential of the proposed procedure, we performed a specific analysis on two representative areas of Catania, the Stesicoro square and San Nullo district (Figure 11), where we estimated the daily and night atmospheric temperatures (Figure 12) and the temperature difference with respect to the suburban and rural areas, ΔTu-r.

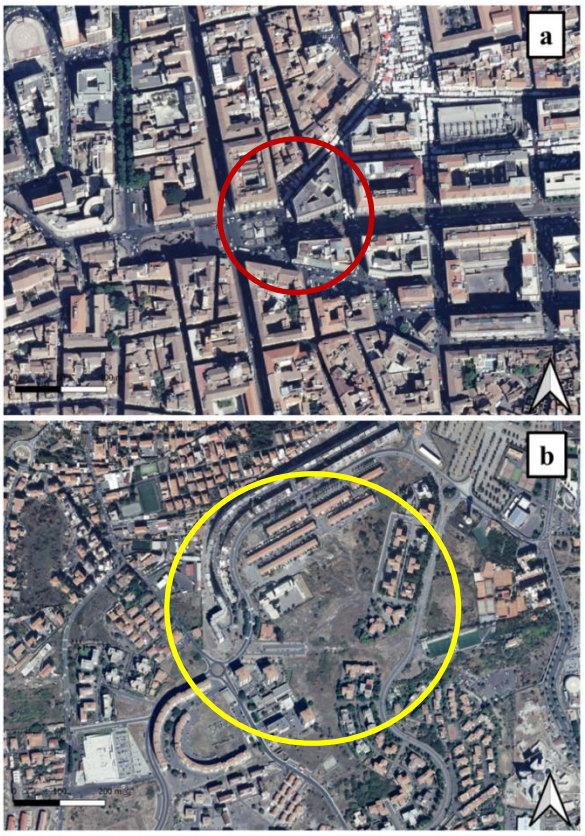

Figure 11. Location of Stesicoro square (red circle in (**a**)) and San Nullo district (yellow circle in (**b**)).

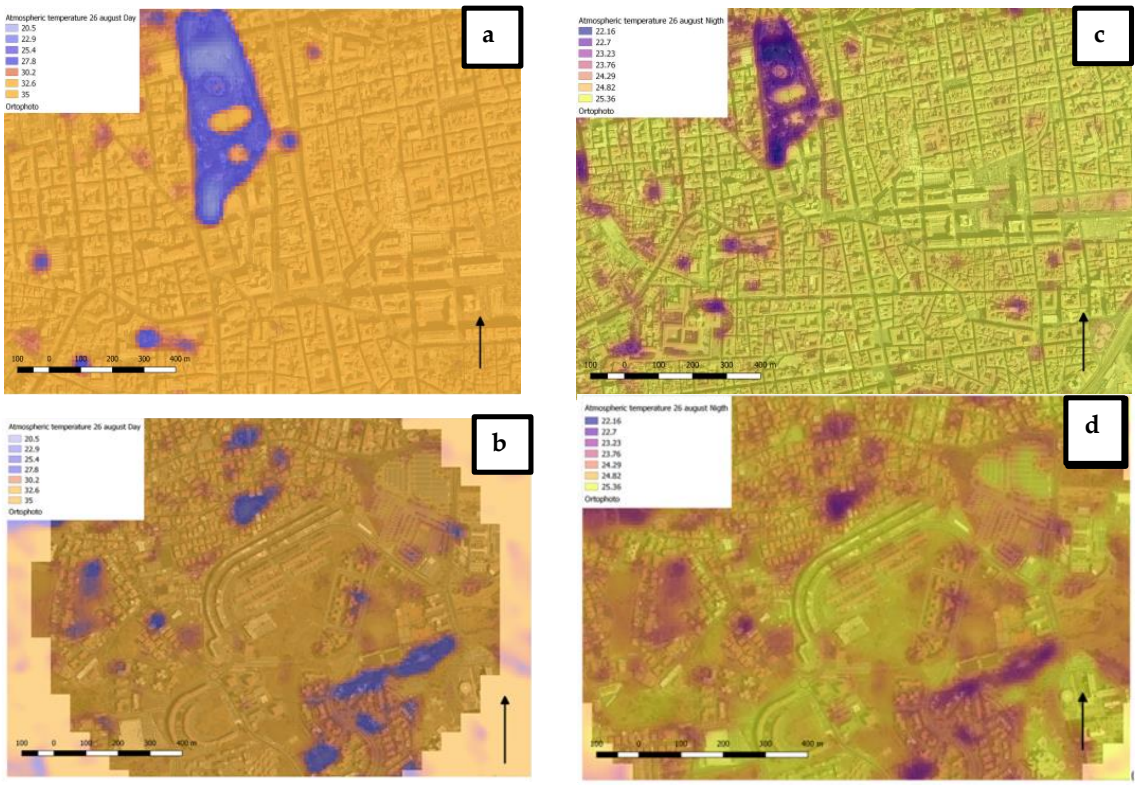

Figure 12. Daily atmospheric temperature in Stesicoro square (**a**) and San Nullo District (**b**), night atmospheric temperature in Stesicoro square (**c**) and San Nullo District (**d**).

For the Stesicoro Square (SteS), ΔTu-r was determined by the differences between Tmin and Tmin in the suburban area of WS2 and the rural area of WS3. In the same way, ΔTu-r for San Nullo (SanN) was determined by the differences between Tmin at San Nullo and Tmin at WS2 and WS3. The atmospheric temperatures at the four locations SteS, SanN, WS2 and WS3 during the nighttime are reported in Figure 13. The two urban districts SteS and SanN have similar atmospheric temperatures for both days, which are about 22.5 °C on 14 July and 25.5 °C on 26 August, while the suburban area, WS2, and the rural area WS3, have meaningful differences. WS2 has a temperature of about 19.9 °C on 14 July and 18.7 °C on 26 August; WS3 has a temperature of about 21 °C on 14 July and 21.6 °C on 26 August.

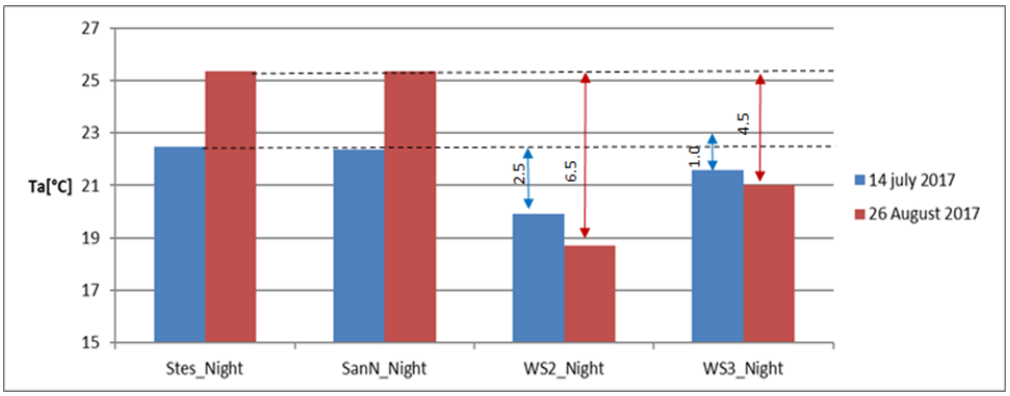

Figure 13. Night time temperature at Stesicoro (Stes), San Nullo (SanN), WS2 and WS3.

Assuming the WS2 location as reference for the rural area, a ΔTu-r of 6.5 °C can be observed. Conversely, assuming the WS3 location as reference, a ΔTu-r of 2.5° is obtained.

This result is coherent with the location of WS2, which is placed closest to the city centre with respect to WS3.

4. Discussion

This work presents a novel procedure to evaluate and analyse the variation of the urban microclimate within cities. The procedure is based on the integration of free and open-source GIS software and satellite remote sensing images freely downloadable from Internet and/or GIS tools. In particular, we used the principle of "Disaggregation of thermal images" and the Kloog's algorithm [48] for the estimation of the land surface temperature and the atmospheric temperature, which allows evaluating the microclimate in urban areas with different built-up densities. The outcome of the procedure are raster maps at high spatial resolution (10 m) that can be inspected by using specific GIS functionaties to perform statistical analyses. This allows obtaining detailed information about the local microclimate, which could provide a valid support tool for assistance in various decision-making processes and city planning. The proposed procedure has been tested using the city of Catania as case study. However, the procedure has been designed to be replicated in any territory for which georeferenced maps and satellite images are available.

We used MODIS and Sentinel-2 satellite images characterized by clear sky conditions and data acquired by weather stations on 12 days between July and August 2017 were used to evaluate the urban climate inside the city of Catania. By looking at the NDVI and LST maps with a spatial resolution of 10 m for the entire investigated period both during daytime and nighttime in the entire urban area, we found that the green areas have temperatures lower than 17 °C during daylight and 2–3 °C during nighttime. By focusing on the sample area shown in Figure 7, the LST_{10} reports a minimum value of 26.05 °C and a maximum value of 44.92 °C. In contrast, the LST estimated from low-resolution images in the same area covers a single pixel with a unique temperature value of 44 °C.

The availability of data on land surface and air temperatures can support studies on the building energy fluxes and outdoor human comfort. In particular, it will be possible to discover the urban areas where the risk due to thermal stresses could be larger and vice versa the urban areas where such kinds of risks are limited, for example during heatwaves phenomena. Moreover, this study could be useful in interventions of urban regeneration as it allows identifying the areas characterized by the worst condition for the outdoor thermal comfort.

The reliability of these results is confirmed by the data acquired by the three different weather stations located in different part of the city, using a methodology already consolidated in literature [49]. Indeed, ΔTu-r, calculated using the weather stations observations, results about 5 °C, while the one derived by satellite ranges between 4.5 and 5.5 °C. Our results are coherent with those obatained by other studies conducted in other cities of the Mediterranean Area, as Bari (Italy) [33], Rome (Italy) [49], Thessaloniki (Greece) [50], Athens (Greece) and Patras (Greece) [51].

The comparison between measured and simulated air temperature highlighted a maximum difference of 2.31 °C. This impreciseness of the prediction is in accordance with the average error, evaluated in the application of Equation (7) as previously pointed out. Although, the average differences between measured and simulated data are less than 1 °C, it is mandatory to extend the number of observations, both in space and time, with the aim of tuning the regression coefficients of Equation (7), in such a way to derive a new correlations validated within the investigated area. Another fundamental aspect that has to be considered is the delay time which relates the time variation of LST and atmospheric temperature due to the rapid change of LST in comparison with atmospheric temperature.

Future work will include the improvement and the validation of the algorithm for the calculation of atmospheric temperatures. This will be achieved by analyzing longer periods and/or using a greater number of "reliable" weather stations uniformly distributed in the area where the microclimate is analyzed to better find the right correlation.

Author Contributions: Conceptualization, A.G., M.M. and G.M.; Investigation, A.G., M.M. and G.M.; Methodology, A.G. and M.M.; Resources, G.M.; Software, M.M.; Writing—Original Draft, A.G., M.M. and G.M. All authors have read and agreed to the published version of the manuscript.

Funding: This work has been partially funded by the University of Catania within the project "Piano Triennale della Ricerca 2020–2022" of the Department of Civil Engineering and Architecture.

Data Availability Statement: Weather stations data were downloaded from the website http://www.sias.regione.sicilia.it/, accessed on 7 July 2020.

Acknowledgments: The authors acknowledge NASA for MODIS data and Copernicus for Sentinel 2 imagery. Thanks are due to Fabio Favazza, whose Master's thesis (supervised by A. Gagliano and M. Mangiameli) inspired this work. We are grateful to the Agro Meteorological Service of Sicilia Region (SIAS), Enel Greenpower and the Department of Electric, Electronics and Computer Engineering of the University of Catania for giving us the possibility to utilize their observed weather data for the examined period. We thanks the three reviewers and the Editor for their comments and suggestions that greatly improved the original version of the manuscript.

Conflicts of Interest: The authors declare no conflict of interest.

References

1. Zeng, Y.; Huang, W.; Zhan, F.B.; Zhang, H.; Liu, H. Study on the urban heat island effects and its relationship with surface biophysical characteristics using MODIS imageries. *Geo Spat. Inf. Sci.* **2010**, *13*, 1–7. [CrossRef]
2. Shahmohamadi, P.; Che-Ani, A.I.; Etessam, I.; Maulud, K.N.A.; Tawil, N.M. Healthy environment: The need to mitigate urban heat island effects on human health. *Proc. Eng.* **2011**, *20*, 61–70. [CrossRef]
3. Heaviside, C.; Macintyre, H.; Vardoulakis, S. The urban heat island: Implications for health in a changing environment. *Curr. Environ. Health Rep.* **2017**, *4*, 296–305. [CrossRef] [PubMed]
4. Gagliano, A.; Nocera, F.; Aneli, S. Computational fluid dynamics analysis for evaluating the urban heat island effects. *Energy Procedia* **2017**, *134*, 508–517. [CrossRef]
5. Cascone, S.; Catania, F.; Gagliano, A.; Sciuto, G. A comprehensive study on green roof performance for retrofitting existing buildings. *Build. Environ.* **2018**, *136*, 227–239. [CrossRef]
6. Jiang, D.; Huang, S.; Han, D. Monitoring and modelling terrestrial ecosystems response to climate change. *Adv. Meterology* **2014**, *2014*, 374987. [CrossRef]
7. Ahmed, S. Assessment of urban heat islands and impact of climate change on socioeconomic over Suez governorate using remote sensing and GIS techniques. *Egypt. J. Remote Sens. Space Sci.* **2018**, *21*, 15–25. [CrossRef]
8. Unger, J. Connection between urban heat island and sky view factor approximated by a software tool on a 3D urban database. *Int. J. Environ. Pollut.* **2009**, *36*, 59. [CrossRef]
9. U.S. Environmental Protection Agency. Reducing Urban Heat Islands: Compendium of Strategies. Draft. 2008. Available online: https://www.epa.gov/heat-islands/heat-island-compendium (accessed on 21 April 2020).
10. Susca, T.; Gaffin, S.R.; Dell'Osso, G.R. Positive effects of vegetation: Urban heat island and green roofs. *Environ. Pollut.* **2011**, *159*, 2119–2126. [CrossRef]
11. Xie, P.; Wang, H. Potential benefit of photovoltaic pavement for mitigation of urban heat island effect. *Appl. Therm. Eng.* **2021**, *191*, 116883. [CrossRef]
12. Li, H.; Harvey, J.T.; Holland, T.J.; Kayhanian, M. The use of reflective and permeable pavements as a potential practice for heat island mitigation and storm water management. *Environ. Res. Lett.* **2013**, *8*, 015023. [CrossRef]
13. Mohajerani, A.; Bakaric, J.; Jeffrey-Bailey, T. The urban heat island effect, its causes, and mitigation, with reference to the thermal properties of asphalt concrete. *J. Environ. Manag.* **2017**, *197*, 522–538. [CrossRef] [PubMed]
14. Cortes, A.; Murashita, Y.; Matsuo, T.; Kondo, A.; Shimadera, H.Y. Numerical evaluation of the effect of photovoltaic cell installation on urban thermal environment. *Sustain. Cities Soc.* **2015**, *19*, 250–258. [CrossRef]
15. Cilek, M.U.; Cilek, A. Analyses of land surface temperature (LST) variability among local climate zones (LCZs) comparing Landsat-8 and ENVI-met model data. *Sustain. Cities Soc.* **2021**, *69*, 102877. [CrossRef]
16. Mutiibwa, D.; Strachan, S.; Albright, T. Land surface temperature and surface air temperature in complex terrain. *IEEE J. Select. Topics Appl. Earth Observat. Remote Sens.* **2015**, *8*, 4762–4774. [CrossRef]
17. Mejbel Salih, M.; Zakariya Jasim, O.; Hassoon, K.I.; Jameel Abdalkadhum, A. Land surface temperature retrieval from LANDSAT-8 thermal infrared sensor data and validation with infrared thermometer camera. *Int. J. Eng. Technol.* **2018**, *7*, 608. [CrossRef]
18. Algretawee, H.; Rayburg, S.; Neave, M. Estimating the effect of park proximity to the central of Melbourne city on Urban Heat Island (UHI) relative to Land Surface Temperature (LST). *Ecol. Eng.* **2019**, *138*, 374–390. [CrossRef]
19. Jin, M.; Dickinson, R.E. Land surface skin temperature climatology: Benefitting from the strengths of satellite observations. *Environ. Res. Lett.* **2010**, *5*, 044004. [CrossRef]
20. Qin, Z.H.; Karnieli, A.; Berliner, P. A mono-window algorithm for retrieving land surface temperature from Landsat TM data and its application to the Israel-Egypt border region. *Int. J. Remote Sens.* **2001**, *22*, 3719–3746. [CrossRef]

21. Otaghsara, M.P.T.; Arefi, H. Modelling urban heat island using remote sensing and city morphological parameters. In Proceedings of the International Archives of the Photogrammetry, Remote Sensing and Spatial Information Sciences, Karaj, Iran, 12–14 October 2019; International Society of Photogrammetry and Remote Sensing (ISPRS): Nice, France, 2019; Volume XLII-4/W18.
22. Mamdouh, E.H.; Amany, S.M.; Lamia, G.E. Monitoring and assessment of urban heat islands over the Southern region of Cairo Governorate. Egypt. *Egypt. J. Remote Sens. Space Sci.* **2018**, *21*, 311–323.
23. Katsoulis, B.D.; Theoharatos, G.A. Indications of urban heat island in Athens, Greece. *Appl. Meteorol.* **1985**, *24*, 1296–1302. [CrossRef]
24. Gagliano, A.; Patania, F.; Nocera, F.; Capizzi, A.; Galesi, A. GIS-based decision support for solar photovoltaic planning in urban environment. In *Sustainability in Energy and Buildings*; Springer: Berlin/Heidelberg, Germany, 2013; pp. 865–874.
25. Mineo, S.; Pappalardo, G.; Mangiameli, M.; Campolo, S.; Mussumeci, G. Rockfall Analysis for Preliminary Hazard Assessment of the Cliff of Taormina Saracen Castle (Sicily). *Sustainability* **2018**, *10*, 417. [CrossRef]
26. Gennaro, A.; Candiano, A.; Fargione, G.; Mangiameli, M.; Mussumeci, G. Multispectral remote sensing for post–dictive analysis of archaeological remains. A case study from Bronte (Sicily). *Archaelogical Prospect.* **2019**, *26*, 299–311. [CrossRef]
27. Gennaro, A.; Candiano, A.; Fargione, G.; Mussumeci, G.; Mangiameli, M. GIS and remote sensing for post-dictive analysis of archaeological features. A case study from the Etnean region (Sicily). *Archeol. Calc.* **2019**, *30*, 309–328. [CrossRef]
28. Mangiameli, M.; Mussumeci, G. Gis approach for preventive evaluation of roads loss of efficiency in hydrogeological emergencies, 2013, International Archives of the Photogrammetry. In Proceedings of the Remote Sensing and Spatial Information Sciences—ISPRS Archives, Padua, Italy, 27–28 February 2013; ISPRS: Nice, France, 2013; Volume 40, pp. 79–87.
29. Mangiameli, M.; Mussumeci, G.; Candiano, A. A low cost methodology for multispectral image classification. In Proceedings of the 18th International Conference on Computational Science and Its Applications, Melbourne, VIC, Australia, 2–5 July 2018; ICCSA: Melbourne, VIC, Australia, 2018; Volume 10964, pp. 263–280.
30. Equere, V.; Mirzaei, P.A.; Riffa, S.; Wang, Y. Integration of topological aspect of city terrains to predict the spatial distribution of urban heat island using GIS and ANN. *Sustain. Cities Soc.* **2021**, *69*, 102825. [CrossRef]
31. Zhou, X.; Okaze, T.; Ren, C.; Cai, M.; Ishida, Y.; Watanabe, H.; Mochida, A. Evaluation of urban heat islandsusing local climate zones and the influence of sea-land breeze. *Sustain. Cities Soc.* **2020**, *55*, 102060. [CrossRef]
32. Bauer, T.J. Interaction of urban heat island e_ects and land–sea breezes during a new york city heat event. *J. Appl. Meteorol. Climatol.* **2020**, *59*, 477–495. [CrossRef]
33. Papanastasiou, D.K.; Melas, D.; Bartzanas, T.; Kittas, C. Temperature, comfort and pollution levels duringheat waves and the role of sea breeze. *Int. J. Biometeorol.* **2010**, *54*, 307–317. [CrossRef]
34. Freitas, E.D.; Rozo, C.M.; Cotton, W.R.; Silva Dias, P.L. Interactions of an urban heat island and sea-breeze circulations during winter over the metropolitan area of São Paulo, Brazil. *Bound. Layer Meteorol.* **2007**, *122*, 43–65. [CrossRef]
35. Martinelli, A.; Kolokotsa, D.D.; Fiorito, F. Urban heat island in Mediterranean coastal cities: The case of Bari (Italy). *Climate* **2020**, *8*, 79. [CrossRef]
36. Kang, X.; Huiping, X. RS and GIS-based analysis of urban heat island effect in Shanghai. In Proceedings of the 18th International Conference on Geoinformatics, Beijing, China, 18–20 June 2010; IEEE: Piscataway, NJ, USA, 2010. [CrossRef]
37. Viana, C.M.; Oliveira, S.; Oliveira, S.C.; Rocha, J. Land Use/Land Cover Change Detection and Urban Sprawl Analysis. In *Spatial Modeling in GIS and R for Earth and Environmental Sciences*; Elsevier: Amsterdam, The Netherlands, 2019; pp. 621–651. [CrossRef]
38. Baghdadi, N.; Mallet, C.; Zribi, M. *QGIS and Applications in Agriculture and Forest*; Wiley Blackwell: Hoboken, NJ, USA, 2018; Volume 3, pp. 1–270. [CrossRef]
39. Li, Z.L.; Tang, B.H.; Wu, H.; Ren, H.; Yan, G.; Wan, Z.; Trigo, I.F.; Sobrino, J.A. Satellite-derived land surface temperature: Current status and perspectives. *Remote Sens. Environ.* **2013**, *131*, 14–37. [CrossRef]
40. Sobrino, J.A.; ElKharraz, J.; Li, Z.L. Surface temperature and water vapour retrieval from MODIS data. *Int. J. Remote Sens.* **2003**, *24*, 5161–5182. [CrossRef]
41. Pettorelli, N. *The Normalized Difference Vegetation Index*; Oxford University Press: Oxford, UK, 2013.
42. Bisquert, M.; Sánchez, T.; Juan, M.; Caselles, V. Evaluation of Disaggregation Methods for Downscaling MODIS Land Surface Temperature to Landsat Spatial Resolution in Barrax Test Site. *IEEE J. Sel. Top. Appl. Earth Obs. Remote Sens.* **2016**, *9*, 1430–1438. [CrossRef]
43. Liu, S.; Su, H.; Zhang, R.; Tian, J.; Wang, W. Estimating the surface air temperature by remote sensing in Northwest China using an improved advection-energy balance for air temperature model. *Adv. Meteorol.* **2016**, *2016*, 11. [CrossRef]
44. Alqasemi, A.S.; Hereher, M.E.; Al-Quraishi, A.M.F.; Saibid, H.; Aldahan, A.; Abuelgasim, A. Retrieval of monthly maximum and minimum air temperature using MODIS aqua land surface temperature data over the United Arab Emirates. *Geocarto Int.* **2020**, *767*, 144330. [CrossRef]
45. Kloog, I.; Nordio, F.; Coull, B.A.; Schwartz, J. Predicting spatiotemporal mean air temperature using MODIS satellite surface temperature measurements across the Northeastern USA. *Remote Sens. Environ.* **2014**, *150*, 132–139. [CrossRef]
46. City of Cambridge. *Massachusetts Climate Change Vulnerability Assessment November 2015*; Appendix D: Urban Heat Island Protocol for Mapping Temperature Projections; City of Cambridge: Cambridge, MS, USA, 2015.
47. Colston, J.M.; Ahmed, T.; Mahopo, C.; Kang, G.; Kosek, M.; de Sousa, F., Jr.; Shrestha, P.S.; Svensen, E.; Turab, A.; Zaitchik, B. Evaluating meteorological data from weather stations, and from satellites and global models for a multi-site epidemiological study. *Environ. Res.* **2018**, *165*, 91–109. [CrossRef]

48. Giannaros, T.M.; Melas, D. Study of the urban heat island in a coastal Mediterranean City: The case study of Thessaloniki, Greece. *Atmos. Res.* **2012**, *118*, 103–120. [CrossRef]
49. Battista, G.; Evangelisti, L.; Guattari, C.; Vollaro, E.D.L.; Vollaro, R.D.L.; Asdrubali, F. Urban Heat Island Mitigation Strategies: Experimental and Numerical Analysis of a University Campus in Rome (Italy). *Sustainability* **2020**, *12*, 7971. [CrossRef]
50. Georgakis, C.; Santamouris, M. Determination of the Surface and Canopy Urban Heat Island in AthensCentral Zone Using Advanced Monitoring. *Climate* **2017**, *5*, 97. [CrossRef]
51. Giannopoulos, A.; Caouris, Y.G.; Souliotis, M.; Sntamouris, M. Characteristics of the urban heat island effect, in the coastal city of Patras, Greece. *Int. J. Sustain. Energy* **2021**, *0*, 1–16. [CrossRef]